Instability of a free shear layer in the vicinity of a viscosity-stratified layer

KIRTI CHANDRA SAHU[1]† AND RAMA GOVINDARAJAN[2]

[1]Department of Chemical Engineering, Indian Institute of Technology Hyderabad, Yeddumailaram 502 205, India

[2]TIFR Centre for Interdisciplinary Sciences, Tata Institute of Fundamental Research Narsingi, Hyderabad 500075, India

(Received ?; revised ?; accepted ?. - To be entered by editorial office)

The stability of a mixing layer made up of two miscible fluids, with a viscosity-stratified layer between them, is studied. The two fluids are of the same density. It is shown that unlike other viscosity stratified shear flows, where species diffusivity is a dominant factor determining stability, species diffusivity variations over orders of magnitude do not change the answer to any noticeable degree in this case. Viscosity stratification, however, does matter, and can stabilize or destabilize the flow, depending on whether the layer of varying velocity is located within the less or more viscous fluid. By making an inviscid model flow with a slope change across the "viscosity" interface, we show that viscous and inviscid results are in qualitative agreement. The absolute instability of the flow can also be significantly altered by viscosity stratification.

1. Introduction

A mixing layer, or a free-shear layer, forms between parallel streams of fluid moving at different velocities and placed adjacent to each other. Viscosity creates this layer of shear, which widens as one moves downstream. The downstream growth is however very slow at high Reynolds numbers, and this flow may, to a very good approximation, be treated as a parallel flow. This flow displays the Kelvin-Helmholtz instability, which becomes non-linear at longer times, and then wraps up the mixing layer into the so-called cats-eye structures. In geophysical situations, one often encounters such shear layers in proximity with stratified layers. Turbidity currents [Nasr-Azadani & Meiburg (2014); Nasr-Azadani *et al.* (2013)] are a good example, a schematic of which is shown in figure 1. An underwater avalanche carrying particulate matter would cause such a current, where a fast flowing particle-laden layer lies below a relatively calm layer of clear water. Between the two, a shear layer develops. At early times, the viscosity (and density) is stratified across the same layer as well, apart from the velocity. The particles, which are slightly more dense than the water, sink slowly so that at later times, the viscosity-stratified layer lies below the shear layer. To consider another situation, viscosity in the ocean increases as a function of depth, and, since it is sensitive to both pressure and temperature, sometimes in opposite senses, contains layers of relatively large viscosity variation. These layers need not, and often do not, coincide with the shear layer. The upper layers of the ocean frequently contain a well-mixed layer of relatively low salinity and higher temperature lying above a layer of higher salinity and lower temperature, as shown in figure 2. We thus have a quiescent stratified layer at some depth. When a river effluxes its waters at the surface of the ocean, we have again a shear layer lying above the stratified layer. It

† Email address for correspondence: ksahu@iith.ac.in

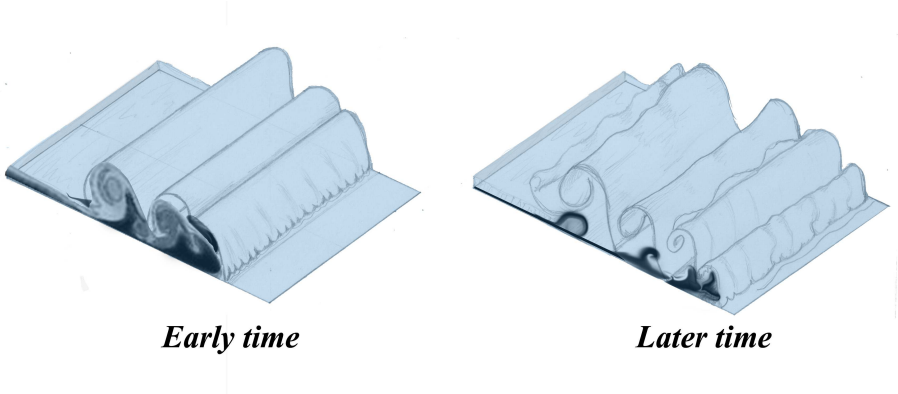

FIGURE 1. Schematic of a shear layer overlying a stratified layer, in a turbidity current. This schematic is representative of a lock-exchange flow [Nasr-Azadani & Meiburg (2014); Nasr-Azadani *et al.* (2013)], where a current of particle-laden water flows below a still layer of clear water. At early times the clear-turbid stratified interface coincides with the shear layer, but as time progresses, the particles sink, such that the stratified layer lies below the shear layer.

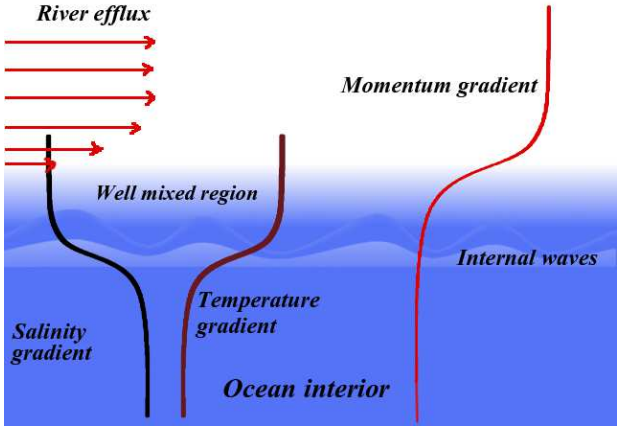

FIGURE 2. Schematic of a portion of the upper layers of an ocean, close to the mouth of a river. The ocean contains a layer of stratification at some depth and the efflux from the river creates a shear layer above it. The concentration in the lower regions is depicted here as constant but is in fact more often a slowly increasing function of depth.

is our purpose in this paper to study the effect on flow stability of the shear layer due to the stratified layer in its proximity. We neglect density effects and only study viscosity effects, because density effects on stability are easy to predict, namely that a layer of lower density lying above one of higher density is stabilizing, whereas the opposite is destabilizing. More important, density effects on stability have been studied extremely widely, whereas viscosity effects, which are often as strong, and more often neglected. It is our objective to bring these effects to the foreground. The combination may be useful to study at a later stage.

We first selectively discuss the literature on a simple shear layer followed by that on stratified shear layers. Betchov & Szewczyk (1963) were the first to study the linear stability of this flow in the viscous regime. They found that the mixing layer is unstable to infinitesimally small disturbances at any Reynolds number. Since then this problem has

been studied by several authors; see for instance Huerre & Rossi (1998); Drazin & Reid (1985) and references therein. Bhattacharya *et al.* (2005) revisited this problem and conducted a linear stability analysis including the non-parallel effects, i.e., the streamwise variation of the basic state. They showed that the flow, as it should be, is stable for small Reynolds numbers, and that this is the primary effect of flow non-parallelism. At larger Reynolds numbers, the parallel flow approximation is shown to be good enough to predict instability. Huerre & Monkewitz (1985) studied a parallel free shear flow in the inviscid limit, and distinguished regimes of absolute and convective instability. Distinguishing between the two has significant consequences for flow dynamics, since an absolutely unstable system, disturbances amplify in the original location, and propagate both downstream and upstream. They can generate a global mode which can dominate large portions of the flow and the system behaves as a self-sustained resonator, while in a convectively unstable flow, disturbances amplify, but are swept away downstream by the basic flow. Huerre & Monkewitz (1985) define a non-dimensional number, $R_t = (U_\infty - U_{-\infty})/(U_\infty + U_{-\infty})$ where U_∞ and $U_{-\infty}$ are the velocities of the two streams, which determines the strength of the mixing layer. Thus $R_t < 1$ and $R_t > 1$ represent mixing layers where the streams are co-current and counter-current, respectively. They demonstrated that free shear flow is absolutely unstable if $R_t > 1.315$, i.e., the counter-current flow is sufficiently strong. The effects of confinement on the stability of shear flow, and the nature of such instabilities have been studied by several authors (for instance, see Juniper (2006); Healey (2009) and relevant references therein). Compressible mixing layers and their stability also have been studied by Robinet & Dussauge (2001). These are not the subjects of the present paper.

To mention a few notable studies on other geometries where the viscosity was not the same everywhere in the flow: in Couette and plane Poiseuille flow. Yih (1967) was the first to study the long wave instability arising due to a viscosity interface. He showed that the flow becomes unstable at any Reynolds number. Several authors (Hooper & Boyd 1983; Hinch 1984) have extended this problem to the short-wave regime in bounded and unbounded flows. In these and several other studies, a viscosity jump was prescribed across the interface. Wilson & Rallison (1999) asked what happens when viscosity is stratified across a thin layer rather than as a step function. They found that a smearing out of the interface has a large stabilizing effect. They had neglected species diffusion, whereas Ern *et al.* (2003) included this effect too. The latter study confirmed that increasing the interface thickness has a stabilizing effect. Secondly when the species are allowed to diffuse into each other, there is again a large stabilizing effect.

Returning to mixing layers, Carpenter *et al.* (2010) studied the density stratified shear layer by conducting a linear stability analysis. The only earlier studies, to the best of our knowledge, which consider a change in viscosity in the vicinity of the mixing layer are those of Boeck & Zaleski (2005); Yecko & Zaleski (2005); Bague *et al.* (2010). They used error function profiles to describe the velocity in each layer. The emphasis was on the air-water interface, so a location of sharp change in viscosity was considered rather than a diffuse viscosity-stratified layer. Secondly since both density and viscosity changed by large amounts across this layer, the effects of viscosity stratification were not isolated. It is well known that a continuous layer of viscosity stratification, even if thin, is very different from a sharp viscosity interface (Govindarajan & Sahu 2014), especially with reference to stability behavior in wall-bounded flows at low Reynolds numbers. In many physical systems, the two fluids under consideration are at least slightly miscible, and it is the former which occurs. Such a viscosity-stratified layer can have a profound effect on the flow dynamics. This is the subject of the present study. Secondly we allow for

the shear layer and the viscosity stratified layer to be separated from each other, as is relevant for the geophysical examples discussed above.

We thus investigate the linear stability characteristics of a shear layer of two miscible, Newtonian and incompressible fluids of equal density and different viscosities by conducting a temporal and spatio-temporal stability analysis. In the present study, a Blasius-type mean equation, modified to include viscosity stratification, is solved to get the base state velocity profile. A Briggs (1964) type approach is used to distinguish convective and absolute instability. We show that the effect of viscosity stratification on the stability of mixing layer is different from that on other shear flows. Diffusivity is known to have a significant effect in other shear flows (Govindarajan & Sahu 2014), but in the mixing layer it is found that the diffusivity of one species into the other makes no difference to the result. This in an indication that the mechanism by which viscosity stratification acts could be inviscid, via a change in the slope of the velocity profile above and below the stratified layer. We show that a mixing layer can be further destabilized by a suitable choice of viscosity ratio, but more interestingly, can be stabilized, when the layer of varying velocity is located within the less viscous region. This is true for both convective and absolute instability.

The rest of the paper is organized as follows. The details of the problem formulation of the basic state and the linear stability analysis are provided in Section 2; the results are discussed in Section 3, and concluding remarks are given in Section 4.

2. Formulation

The linear stability of a shear layer made up of two miscible, Newtonian and incompressible fluids of equal density and different viscosities is studied. As shown in figure 3, the two fluids are separated by a mixed layer of uniform thickness, q, with fluid '1' and fluid '2' occupying the regions $-\infty < y < -h-q$ and $-h < y < \infty$, respectively. In prescribing the thickness q to be uniform, we have employed the parallel flow approximation. Two fluids which meet at an interface diffuse into each other at a rate proportional to the inverse of the Péclet number $Pe = ScRe$. The downstream growth of the interface is thus small at high Reynolds number, and since we are working at Reynolds numbers of $O(10^2)$, the parallel flow approximation is justified unless $Sc << 1$. The two fluids contain different concentrations s of a (scalar) solute. Without loss of generality, s is taken to be 0 in the bottom layer, and 1 in the top layer, such that the viscosity of the fluids in the bottom and top layers are μ_1 and μ_2, respectively. The Cartesian coordinate system is used to formulate the problem, where x and y denote the coordinates in the horizontal and the vertical directions, respectively. The effect of gravity is neglected in this study.

The viscosity, μ, is modeled as an exponential function of the scalar s:

$$\mu = \mu_1 \exp(sR_s), \tag{2.1}$$

where $R_s\,(\equiv \ln(\mu_2/\mu_1))$ is the log-mobility ratio of the scalar.

The following scaling is employed to render the governing equations dimensionless:

$$(x, y, q, h) = \delta\left(\widetilde{x}, \widetilde{y}, \widetilde{q}, \widetilde{h}\right),\ t = \frac{\delta}{\Delta U}\widetilde{t}, \tag{2.2}$$

$$(u, v) = \Delta U(\widetilde{u}, \widetilde{v}),\ p = \rho(\Delta U)^2\widetilde{p},\ \mu = \widetilde{\mu}\mu_1, \tag{2.3}$$

where the tildes designate dimensionless quantities; $\Delta U(\equiv U_\infty - U_{-\infty})$ denotes the velocity scale; δ represents the mixing layer thickness; u and v are the velocity components in the x and y directions, respectively; ρ is the constant density; t is time and p denotes

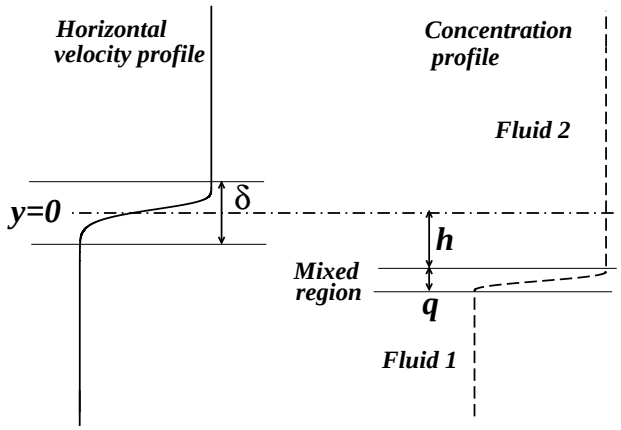

FIGURE 3. Schematic of the flow; the solid and the dashed line represent the horizontal velocity and concentration profiles in the vertical direction, respectively. Fluids '1' and '2' occupy the bottom ($-\infty < y < -h-q$) and top ($-h < y < \infty$) layers, respectively. The two fluids are separated by a mixed layer of uniform thickness q. δ represents the mixing layer thickness, defined as $y|_{0.99U_{-\infty}} - y|_{0.99U_{\infty}}$, where U_{∞} and $U_{-\infty}$ are the free streamvelocity at $y \to -\infty$ and $y \to \infty$, respectively.

pressure. Now dropping the tildes for convenience, the dimensionless governing equations are given by

$$\nabla \cdot \mathbf{u} = 0, \tag{2.4}$$

$$\left[\frac{\partial \mathbf{u}}{\partial t} + \mathbf{u} \cdot \nabla \mathbf{u}\right] = -\nabla p + \frac{1}{\mathrm{Re}} \nabla \cdot \left[\mu(\nabla \mathbf{u} + \nabla \mathbf{u}^T)\right], \tag{2.5}$$

$$\frac{\partial s}{\partial t} + \mathbf{u} \cdot \nabla s = \frac{1}{\mathrm{ScRe}} \nabla^2 s, \tag{2.6}$$

where $\mathbf{u}$ is the velocity vector, $\mathrm{Re}(\equiv \rho \Delta U \delta / \mu_1)$ and $\mathrm{Sc}(\equiv \mu_1 / \rho \mathcal{D})$ are the Reynolds number and Schmidt number, respectively, wherein $\mathcal{D}$ is the diffusion coefficient of the scalar.

2.1. *Base state*

The base state, about which linear stability characteristics will be analyzed, corresponds to a steady, parallel, fully-developed flow, where $V = 0$ and U is a function of y alone. Upper-case letters are used to designate the base state. We use a simple model base flow, and also one obtained from a numerical simulation of the Navier-Stokes equations. The model base state concentration profile is described by

$$S = \frac{1}{2}\left[\tanh\left\{\frac{4.595}{q}\left(y - h - q/2\right)\right\} + 1\right], \tag{2.7}$$

such that the concentration and its derivative are continuous everywhere inside the domain. The tanh profile is chosen here since several authors (Ern *et al.* 2003; Sahu *et al.* 2009) have used it in this kind of flow stability problem, and also it is the standard form used in binary-fluid computations, but any sufficiently smooth profile can be used instead and the answers will not change. If two fluids of different concentration come into contact and slowly diffuse into each other, under the boundary layer approximation they will attain an error function profile for the concentration. Such a profile is shown to be indistinguishable from the tanh profile in figure 4 below and therefore the instability results in the two cases are the same. The constant in the above equation is selected so

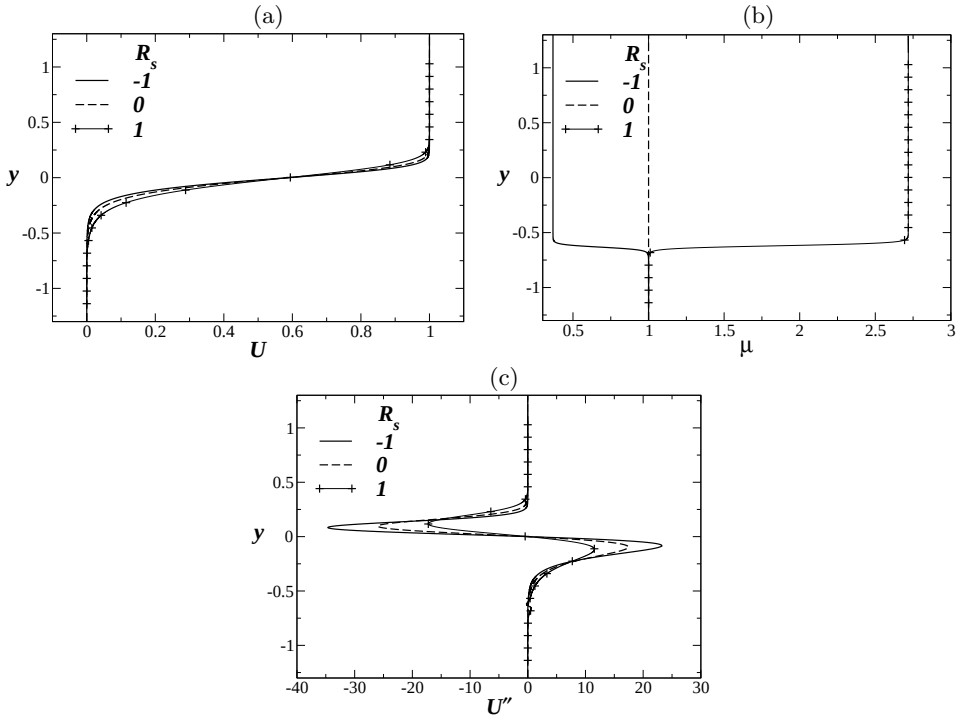

FIGURE 4. Typical basic steady-state profiles of (a) U, (b) μ_0 and (c) U'', for different values of R_s. The other parameters are chosen as $h = 0.569$, $q = 0.1138$ and $R_t = 1$. The dotted lines with filled triangles in panel (a) and (b) represent the profiles obtained from the direct numerical simulation for $R_s = -1$. It can be seen the results obtained using tanh and error-function profile are indistinguishable, and are both very close approximates of the profile obtained from direct numerical simulations.

as to make S vary between 0.01 and 0.99 in the mixed region ($-h - q \leqslant y \leqslant -h$). The functional dependence of the dimensionless viscosity is given by

$$\mu_0 = e^{(R_s S)}. \tag{2.8}$$

Under the boundary layer approximation, it can be shown (see Appendix A) that the base state velocity profile then satisfies the following Blasius-type profile, modified to include viscosity variation:

$$f''' + \frac{1}{2\mu_0} f f'' + \frac{\mu_0'}{\mu_0} f'' = 0, \tag{2.9}$$

where $f' = U$ and the prime denotes differentiation with respect to y. The boundary conditions used to solve Eq. (2.9) are

$$f = 0, \quad f' = U_{-\infty}/\Delta U \quad \text{at} \quad y = -H, \quad \text{and} \tag{2.10}$$

$$f' = U_{\infty}/\Delta U \quad \text{at} \quad y = H, \tag{2.11}$$

where H is large enough to make the results independent of the choice, up to at least five decimal places.

In figure 4 a,b and c, typical base state profiles of the horizontal velocity (U), viscosity (μ_0) and the second derivative of the horizontal velocity component (U'') are shown for different values of R_s, respectively. The rest of the parameters are chosen as $h = 0.569$, $q = 0.1138$ and $R_t \, [\equiv \Delta U/(U_{\infty} + U_{-\infty})] = 1$. It is seen that the Blasius shear layer is not

top-down symmetric. Note that the length scale, δ is not known *a priori*, we first solve Eq. (2.9) with an arbitrary length scale, find δ, and then re-scale all relevant lengths. For this reason, we have unusual looking numbers for the parameters h and q. A negative (positive) value of R_s represents a situation where the bottom fluid is more (less) viscous, whereas $R_s = 0$ means that both fluids are of equal viscosity. It can be seen in figure 4c that a positive value of R_s makes the velocity profile more gentle. Therefore, we intuitively expect the flow to be stabilized for positive R_s value compared with that for negative value of R_s, and we will find this to be true.

We now perform direct numerical simulations, where we solve Eqs. (2.4)-(2.6) by considering a computational domain of 30×10, and using 601 and 201 grid points in the x and y directions, respectively. A periodic boundary condition is imposed in the x-direction and no-flux boundary conditions for both the concentration and the velocity are used at the boundaries in the y-direction. It is checked that if the no-flux conditions are applied on a bigger domain, the answers do not change significantly. The initial conditions are as follows: the values of the streamwise velocity component is set to zero and one at the bottom and top halves of the domain, respectively. The interface for the concentration lies at the corresponding location for $y = h + q/2$. Again the values of concentration are set to one and zero above and below this line respectively. The reader is referred to Mishra *et al.* (2012) for details of the numerical method used. The dotted lines with filled triangles in panel (a) and (b) represent the profiles obtained from these direct numerical simulations for $R_s = -1$ Sc $= 100$, Re $= 100$ and $t = 80$. It is clear that the model mean flow profiles are a very good approximation of the exact profiles.

2.2. *Linear stability analysis*

We examine the temporal and spatio-temporal linear stability of the base flow given by Eqs. (2.7)-(2.9) using a normal modes analysis. For comparison, we also include the stability analysis of a numerically obtained base flow. Given that Schaflinger (1994); Yih (1955) showed that Squire's theorem applies in viscosity-stratified flows as well, we are assured that two-dimensional perturbations become unstable at a lower Reynolds number than three-dimensional ones. We therefore restrict ourselves to two-dimensional perturbations. In the standard way (e.g. see for instance Schmid & Henningson (2001)) flow variables are split into base state quantities and two-dimensional perturbations, designated by a hat:

$$(u, v, p, s)(x, y, t) = (U(y), 0, P, S(y)) + (\hat{u}, \hat{v}, \hat{p}, \hat{s})(y)e^{\mathrm{i}(\alpha x - \omega t)}, \tag{2.12}$$

such that a given mode is unstable if $\omega_i > 0$, stable if $\omega_i < 0$ and neutrally stable if $\omega_i = 0$. Here $\mathrm{i} \equiv \sqrt{-1}$, α and $\omega(\equiv \alpha c)$ are the wavenumber and frequency of the disturbance, respectively, wherein c is the phase speed of the disturbance. In temporal stability analysis α and ω are treated as real and complex quantities, respectively, whereas both are complex in spatio-temporal analysis. In Eq. (2.12), the perturbation viscosity is given by

$$\hat{\mu} = \frac{d\mu_0}{dS}\hat{s}. \tag{2.13}$$

The amplitude of the velocity disturbances are then re-expressed in terms of a stream-function $[(\hat{u}, \hat{v}) = (\psi', -\mathrm{i}\alpha\psi)]$. Substitution of Eq. (2.12) into Eqs. (2.4)-(2.6), subtraction of the base state equations, subsequent linearization and elimination of the pressure perturbation yields the following linear stability equations [Govindarajan (2004); Sahu *et al.*

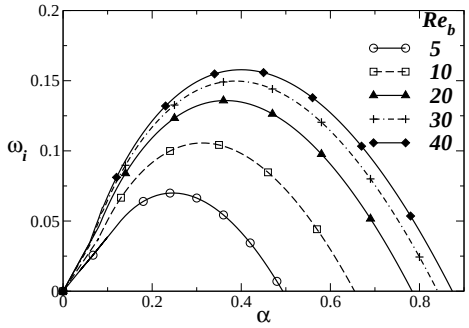

FIGURE 5. Comparison with the dispersion curves (ω_i versus α) of Betchov & Szewczyk (1963) (symbols) for different values of Re_b with present results (lines). Here velocity profile given by $U = U_0 \tanh(y/\delta)$ is used as suggested by Betchov & Szewczyk (1963), and Re_b is defined as $U_0\delta\rho/\mu$. Note Re_b is defined differently from Re.

(2009)], where the hat notation is suppressed:

$$\mathrm{i}\alpha\mathrm{Re}\left[\left(\psi'' - \alpha^2\psi\right)(U-c) - U''\psi\right] = \mu_0\left(\psi^{iv} - 2\alpha^2\psi'' + \alpha^4\psi\right) + 2\mu_0'\left(\psi''' - \alpha^2\psi'\right) + \mu_0''\left(\psi'' + \alpha^2\psi\right) + U'\left(\mu'' + \alpha^2\mu\right) + 2U''\mu' + U'''\mu, \tag{2.14}$$

$$\mathrm{i}\alpha\mathrm{ScRe}\left[(U-c)\,s - \psi s'\right] = \left(s'' - \alpha^2 s\right). \tag{2.15}$$

The boundary conditions at the free streams are

$$\psi = \psi' = s = 0. \tag{2.16}$$

Eqs. (2.14)-(2.15) along with the boundary conditions (2.16) constitute an eigenvalue problem which is discretised using Chebyshev spectral collocation and solved using the public domain software, LAPACK. As gradients are large in the viscosity-stratified region, we require a large number of grid points in this region. For this we use the stretching function [Govindarajan (2004)]

$$y_j = \frac{a}{\sinh(by_0)}\left[\sinh\left\{(y_c - y_0)b\right\} + \sinh(by_0)\right], \tag{2.17}$$

where y_j are the locations of the grid points, a is the mid-point of the stratified layer, y_c is a Chebyshev collocation point,

$$y_0 = \frac{0.5}{b}\ln\left[\frac{1 + (e^b - 1)a}{1 + (e^{-b} - 1)a}\right], \tag{2.18}$$

and b is the degree of clustering. We have taken $b = 8$ which gives an accuracy of at least five decimal places in the range of parameters used.

3. Results and discussion

3.1. *Viscous temporal stability analysis*

To validate our approach we compare present results in figure 5 with those of Betchov & Szewczyk (1963) in the unstratified mixing layer. Just for this figure we prescribe a tanh velocity profile $U = U_0 \tanh(y/\delta)$, the same as one used by Betchov & Szewczyk (1963), and use their scales. The dispersion curves are paraboloidal, with $\omega_i > 0$ over a finite band of wavenumbers, indicating a linear instability. The "most-dangerous", and "cut-off", modes correspond to the values of α for which ω_i is maximal, and beyond which $\omega_i > 0$, respectively. The results presented in this figure are in excellent agreement with

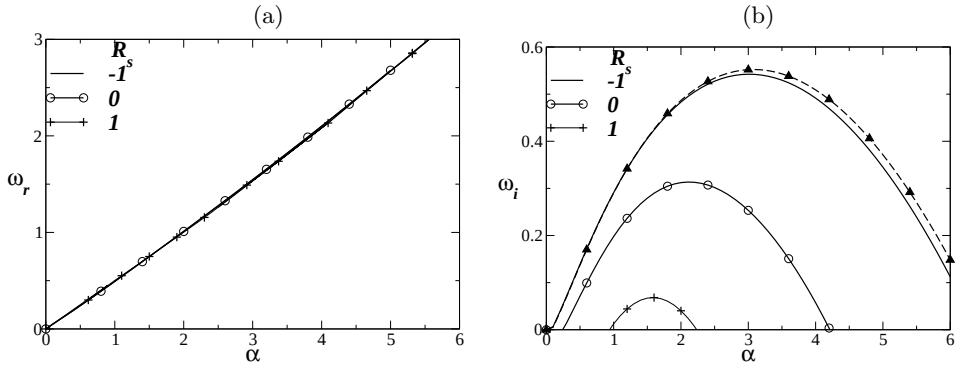

FIGURE 6. The dispersion curves (a) ω_r versus α, (b) ω_i versus α for different values of R_s. The dotted line with filled triangles represents dispersion curve for the base state obtained from the direct numerical simulation for $R_s = -1$. Values of the remaining parameters are Re = 100, Sc = 1, $h = 0.569$, $q = 0.1138$ and $R_t[\equiv \Delta U/(U_\infty + U_{-\infty})] = 1$.

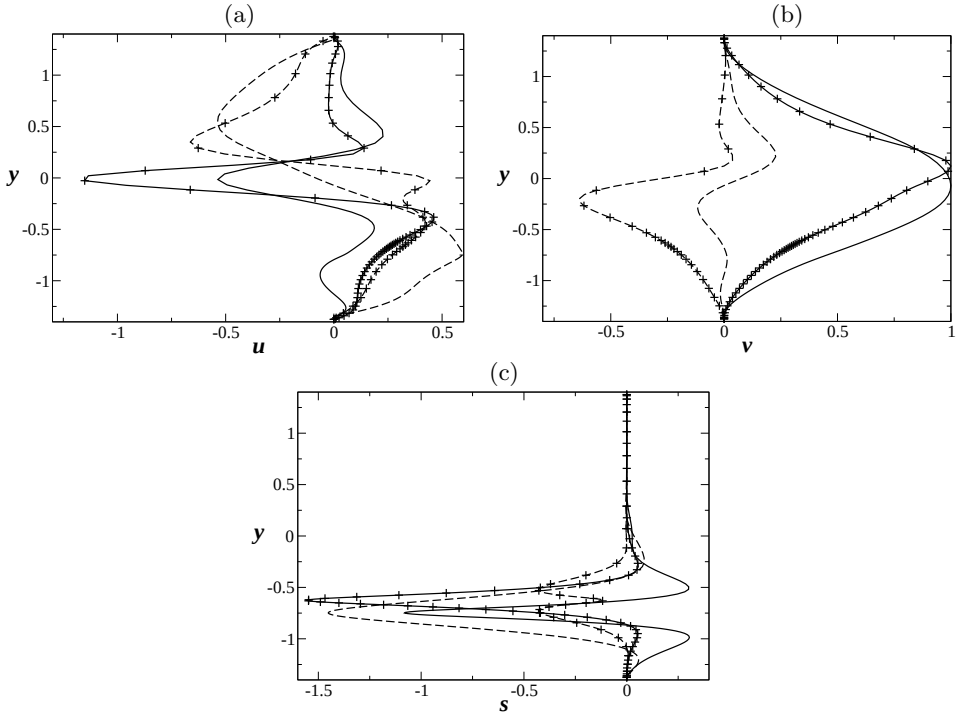

FIGURE 7. Eigenfunctions (a) u, (b) v and (c) s for two different values of R_s at $\alpha = 2.5$. The other parameters are chosen as $h = 0.569$, $q = 0.1138$, Sc = 1 and $R_t = 1$. Solid lines: real parts, dashed lines: imaginary parts, without symbol: $R_s = 0$ and with symbols: $R_s = 1$.

those of Betchov & Szewczyk (1963). They, and several researchers after them, found that the flow is unstable at any Reynolds number. However, Bhattacharya *et al.* (2005) by considering the horizontal variation of the basic state showed that the flow is stable below Reynolds number 30.

How is the instability affected by viscosity stratification? In figure 6, the variation of ω_r and ω_i are plotted as functions of α for different values of R_s. The rest of the parameters are Re = 100, Sc = 0, $h = 0.569$, $q = 0.1138$. The velocity ratio $R_t = 1$, which means

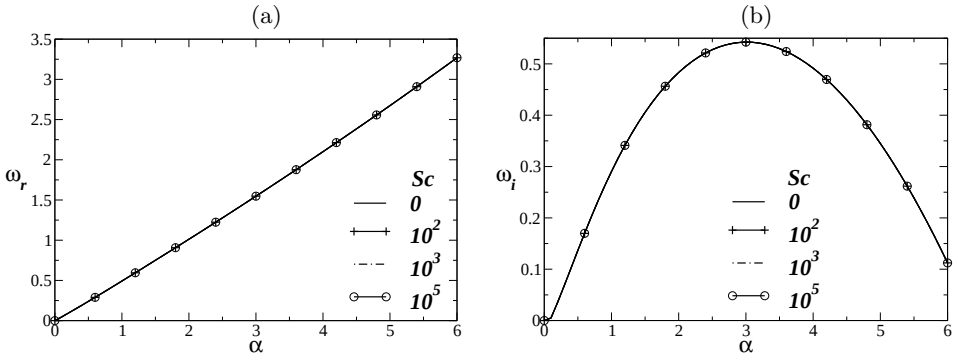

FIGURE 8. The dispersion curves (a) ω_r versus α, (b) ω_i versus α for different values of Sc. The other parameters are Re = 100, $h = 0.569$, $q = 0.1138$, $R_s = -1$ and $R_t = 1$.

that the velocity of the bottom and top layers are 0 and 1, respectively. When the static fluid layer is more viscous ($R_s = -1$) the flow is more unstable than when this layer is less viscous ($R_s = 1$). The growth rate for the unstratified mixing layer ($R_s = 0$) lies in between the two. We also found (not shown) that for $R_s = 2$ the flow is completely stable ($\omega_i < 0$ for all values of α). The growth rate of the instability for the mean flow profiles obtained from direct numerical simulations is shown here by the dotted line with filled triangles. It is clear that the model flow contains the physics of the numerically solved base flow, so we use the model flow to present the rest of the results.

It can be seen in figure 6a that the circular frequency (the real part of ω) varies linearly with the wavenumber, and, unlike the growth rate, is practically independent of the viscosity stratification. It is well-understood that an altered phase gives rise to altered stability, so we examine whether the stabilization and destabilization of the flow is reflected in a modification of the eigenfunctions, especially in the layer of stratified viscosity. That this is so is evident from figure 7, where the eigenfunctions with and without viscosity stratification are shown for a particular wavenumber, $Sc = 1$ and $Re = 100$. The normal component of the disturbance velocity shows both an altered magnitude and altered phase in the viscosity stratified layer (centered around $y = -0.6$). The streamwise component too shows an altered phase. These changes result in a modified phase within the shear layer too, and thus in a changed production. In problems of this type, the numerical value of the answer will depend on the choice of scales used to define the Reynolds number. In particular, while it is usual in viscosity-stratified flows to choose the viscosity of the lower layer as the scale, it may be asked whether the stabilization or destabilization seen is because of this choice. In this case the qualitative nature of the results, i.e. stabilization when the shear layer lies predominantly in the high viscosity regime, is independent of the choice of viscosity scale: whether μ_2 or the arithmetic average of μ_1 and μ_2. We will return to this point later.

We now turn to the effect of changing the diffusivity of the two solutes. Figure 8 shows that the growth rates are practically independent of solute diffusivity. Over a huge range of Schmidt number, the instability is unaltered. This comes as a surprise when one is acquainted with shear flows of many other descriptions, such as channel and pipe flows, boundary layer flows and so on. It is usually the case that decreasing solvent diffusivity (increasing Sc) has a big destabilizing effect (Ern *et al.* (2003); Govindarajan & Sahu (2014) and references therein), and often there are new modes of instability that are peculiar to low diffusivities. The fact that solvent diffusivity does not matter to the stability of this flow is remarkable. How can we explain our finding that while

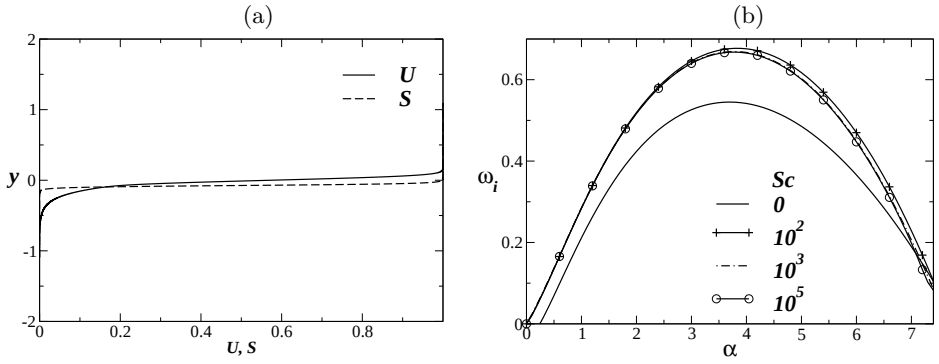

FIGURE 9. (a) The basic state velocity (U) and concentration (S) profiles; (b) ω_i versus α for different values of Sc for $h = 0.0524$ (i.e. when the viscosity stratified layer overlaps with the momentum stratified layer). The other parameters are Re $= 100$, $q = 0.1382$, $R_s = -1$ and $R_t = 1$.

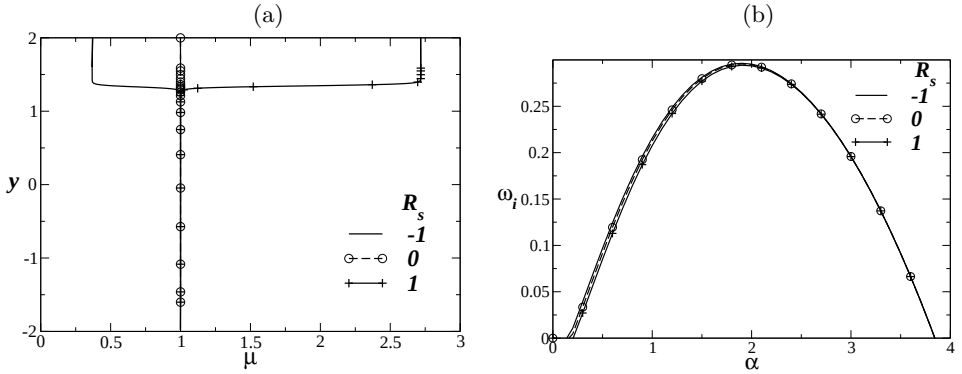

FIGURE 10. (a) Viscosity profile, (b) the dispersion curves ω_i versus α, for different values of R_s. Values of the remaining parameters are Re $= 100$, Sc $= 1$, $h = -1.395$, $q = 0.1138$ and $R_t[\equiv \Delta U/(U_\infty + U_{-\infty})] = 1$.

viscosity stratification does have a significant effect on the stability, the diffusivity does not matter? It could be because viscosity stratification acts on the stability in an 'inviscid' non-diffusive way. We therefore design a model inviscid velocity profile in the next subsection to understand this phenomenon. Another feature to be noted is that in the other geometries, the viscosity perturbation has a very large effect especially when the viscosity stratified layer overlaps with the critical layer of the dominant disturbance mode. In the present case, the critical layer typically lies within the momentum stratified layer. In the case shown, we have $\delta = 1$, $q = 0.1138$ and $h = 0.569$, so the two layers are, for the most part, separated from each other. This will reduce the effect that reduced diffusivity can have.

In figure 9 we present a case where the two layers overlap to a significant degree. It is seen that at low Schmidt numbers, reducing the diffusivity does have a destabilizing effect on the stability, but the effect is far smaller than in wall-bounded flows. This is another indication that an 'inviscid' wave-interaction mechanism is in operation, rather than a critical layer resonance.

This leads to the question of the effect on the stability of the distance between the shear layer and the viscosity stratified layer. First, as per our argument that it is the interaction of the two layers which is important, if the two layers are very far away

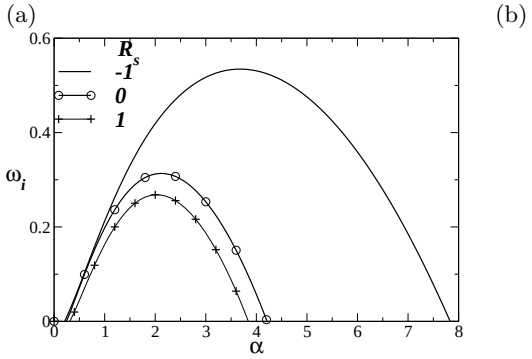

FIGURE 11. Dispersion curves for different values of R_s when $h = 0$, i.e., the centers of the two layers overlap. The remaining parameters are Sc $= 1$, $Re = 100$, $q = 0.1138$ and $R_t = 1$.

from each other, there should be no effect of the viscosity stratification on the stability. This is demonstrated in figure 10, where $h = -1.395$ i.e., the centers of the two layers are separated by more than twice the thickness of the shear layer. In the presence of a distant stratified layer, irrespective of the sense of stratification, the shear layer displays the same stability behavior as in the unstratified case. A negative value of the separation is chosen for this demonstration because this places the shear layer in the lower fluid, and our viscosity scale being that of the lower fluid, this provides a direct comparison. A case worth considering is when the separation distance between the two layers is zero, shown in figure 11. For a negative R_s behavior is similar to that seen earlier at a positive value of h, but the growth rate for positive R_s registers an increase.

Next we plot, in figure 12, the growth rate of the most unstable disturbance, maximized over all wavelengths in each case, as a function of the separation distance. We remark that we neither expect, nor obtain, mirror symmetry of the results in the two figures. We first discuss the solid lines, which are plotted for $Re = 100$. It is seen that stability is a sensitive function of the separation distance. Our conclusion that the flow tends to be stabilized when the shear layer lies in the more viscous fluid, e.g. when $R_s > 0$ and $h > 0$, holds over a range of separation distance. The largest effect of separation distance is seen when the separation distance is small, i.e., the two layers overlap significantly. Both figures 12(a) and (b) make it evident that, for small h, as the centre of the shear layer moves into the layer of lower viscosity, a large stabilization is seen. The fact that viscosity stratification forms a singular perturbation when it overlaps with the critical layer has been shown before in channel flow, see e.g. Ranganathan & Govindarajan (2001); Govindarajan *et al.* (2001) and film flow (Usha *et al.* (2013)) and discussed in detail in Govindarajan & Sahu (2014). In those cases, a small change in the separation distance when the two layers had a overlap made a big difference, sometimes of an order of magnitude, to the stability behavior is observed. The critical layer in a shear flow lies close to the centre ($y = 0$), so at small h, we believe that what we obtain here is another case of this overlap mode of instability. Direct numerical simulations as well as experiments are needed to check this linear stability prediction.

At small h the choice of a viscosity scale does not change the sign of the effect. However at large h we have seen that choosing the viscosity close to the shear layer as the viscosity scale gives a direct comparison between stratified and unstratified flow. Before making a general statement about the sign of destabilization and stabilization as a function of separation we re-examine how the results reflect our choice of viscosity scale. As we have seen, there is no ideal viscosity scale. We have made the simplest choice of that

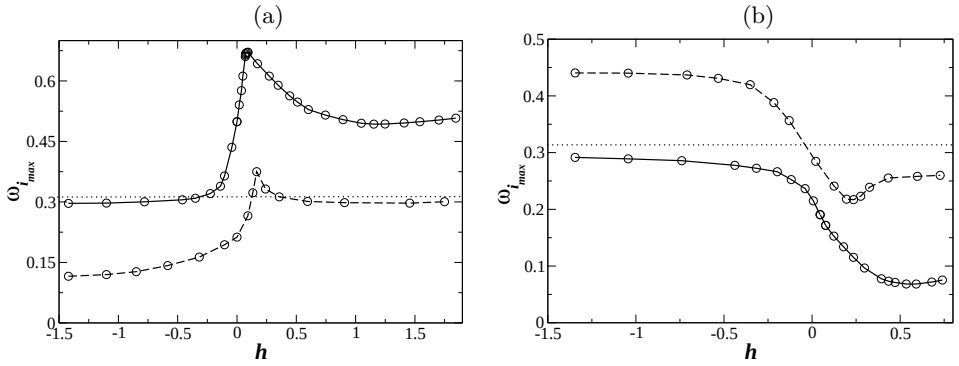

FIGURE 12. Disturbance growth rate ω_{imax} (maximized over all wavenumbers) versus the separation distance h for (a) $R_s = -1$ and (b) $R_s = 1$. The solid lines in both figures are for $Re = 100$. The values of the other parameters are $q = 0.1394$, Sc $= 1$ and $R_t = 1$. The dashed line in (a) is obtained for $R_s = -1$ at a Reynolds number of $100/e$ whereas that in figure (b) is obtained with $R_s = 1$ at $Re = 100e$. The dotted lines ($\omega_{imax} = 0.3138$ and $\omega_{imax} = 0.1105$) in panel (a) show the maximum growth rate in an unstratified shear layer at $Re = 100$ and $Re = 100/e$, respectively. The dotted lines ($\omega_{imax} = 0.3138$ and $\omega_{imax} = 0.4411$) in panel (b) show the maximum growth rate in an unstratified shear layer at $Re = 100$ and $Re = 100e$, respectively.

of one of the fluids. Probably the fairest scale would be an arithmetic average of the two viscosities. However, to make the harshest test of our conclusions, we repeat our calculations in such a way as to make the Reynolds number based on the top viscosity equal to 100, i.e., by using $Re = 100/e$ for $R_s = -1$ and $Re = 100e$ for $R_s = 1$ (where Re is as per our definition). These are respectively shown by the dashed lines in figures 12 (a) and (b). As expected, the flow is more unstable at higher Reynolds number and more stable at lower Reynolds number, but there is no qualitative change in the variation with separation distance. In figure 12(a) the fact that for a range of h (around $h = 0.25$), the viscosity stratified flow at a Reynolds number of just $100/e$ is already more unstable than an unstratified layer at a Reynolds number of 100 makes it evident that viscosity stratification has a destabilizing effect when it interacts with the shear layer. Conversely, when $R_s = 1$ [figure 12(b)], stratified flow at a Reynolds number as high as $100e$ is seen to be more stable than an unstratified shear layer of just $Re = 100$. Finally, in figure 13 we choose the viscosity of the stratified layer at the inflexion point in its velocity profile as a representative viscosity of the shear layer, and compare the maximum growth rate to that of an unstratified layer of that viscosity. Note that this viscosity depends on the separation distance. The effects of stratification are mare more evident in this figure. The best stabilization or destabilization is achieved when the stratified layer overlaps significantly with the shear layer, but their centers are separated somewhat. We may conclude that the stability of shear layer is affected by the presence of viscosity stratification. Locating the shear layer in the less viscous part of the flow is truly destabilizing, irrespective of the choice of viscosity scale, whereas locating it in the more viscous part is stabilizing.

In order to estimate the effect of the thickness of the stratified layer, the variation of ω_i is plotted as functions of α for different values of q in figure 14. It can be seen that increasing the smoothness has a stabilizing influence.

3.2. *Inviscid model: temporal stability*

The objective of this subsection is to demonstrate the similarity between the behaviour we observed above in the viscous case with an inviscid model. It gives credence to the

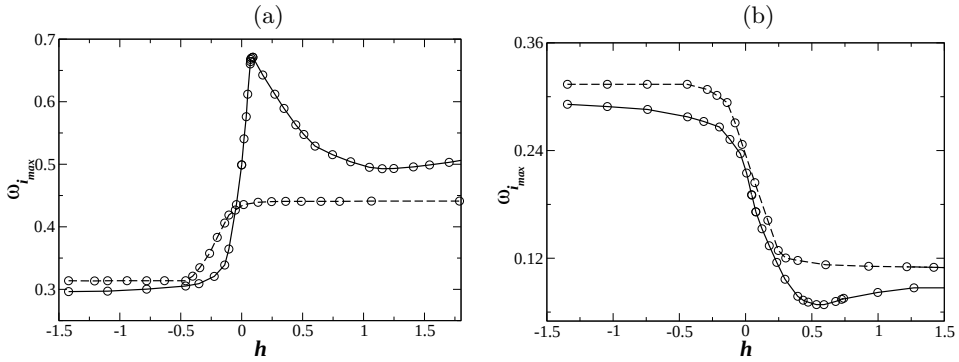

FIGURE 13. Comparison of maximum growth rate in the viscosity stratified case with an unstratified shear layer whose viscosity is adjusted to match that of the stratified layer at its point of inflexion. The disturbance growth rate ω_{imax} is maximized over all wavenumbers in each case. Solid lines: (a) $R_s = -1$ and (b) $R_s = 1$. The dashed lines in both panels show the maximum growth rate in an unstratified shear layer for $Re = 100/\mu_{PI}$, where in μ_{PI} represents the viscosity of the corresponding stratified flow at the point of inflection.

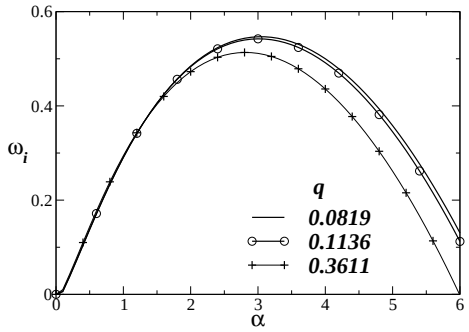

FIGURE 14. The dispersion curves (ω_i versus α) for different values of q. Values of the remaining parameters are Re = 100, Sc = 1, $h = 0.569$, and $R_t[\equiv \Delta U/(U_\infty + U_{-\infty})] = 1$.

surmise that wave-interaction could be operational in both cases, but we note that this does not constitute a proof. Given several differences between this model and the viscous case, numerical comparisons of growth rates are not meaningful.

A famous example of wave-interaction is the Kelvin-Helmholtz (KH) instability. When modeled in terms of a piecewise linear velocity profile, it is seen that the waves on each interface interact to produce the instability, see e.g. Craik (1985); McIntyre (2013); Caulfield (1994); Heifetz & Methven (2005); Heifetz *et al.* (2006); Harnik *et al.* (2006); Bishop & Heifetz (2000); Biancofiore & Gallaire (2012); Boeck & Zaleski (2005). On these lines, we model the velocity profile for the present flow with three interfaces, labelled as 1, 2 and 3, as shown in figure 15(a). The ratio of slopes across the middle interface represents the inverse of the viscosity ratio. As before, the distance of the vorticity interface is measured from the location of average velocity. The formulation of the instability equation for this model is given in appendix B.

In isolation, each of the three interfaces could support neutral modes. However, when allowed to interact, we get instabiity. If the middle interface were absent we would have the standard KH mode, shown by the dashed line in figure 15(b). The three-wave interaction is seen to significantly affect the KH growth rate. At the characteristic wavenumber (or frequency) of the dominant KH mode, instability is enhanced when the layer of varying velocity is located within the higher viscosity region, and suppressed when this

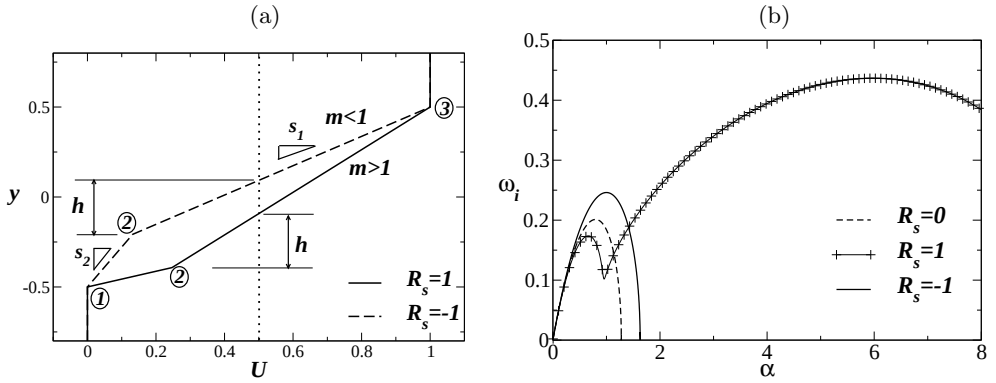

FIGURE 15. (a) Inviscid velocity profile mimicking the effect of viscosity stratification on the base flow. $h = 0.6$, $R_t = 1$. (b) Growth rate of the dominant instability for each of the profiles shown on the left. Here $m = e^{R_s}$.

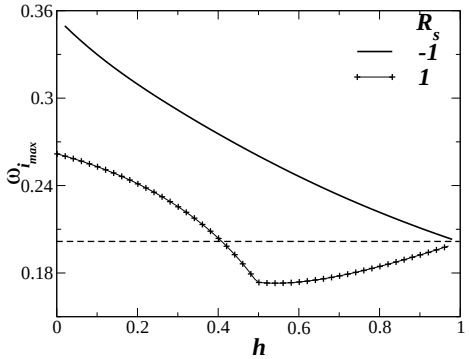

FIGURE 16. The dominant growth rate for the long wave mode as a function of the interface location h. The dashed line indicates the growth rate in the unstratified case. Given the symmetry in the problem, it is sufficient to consider only positive values of h.

layer is within the less viscous region. This is just what happened in the viscous case discussed in the previous section, and the qualitative similarity between the low wavenumber part of figure 15(b) and figure 6(b) is evident. However, there is an additional mode at high wavenumbers (short wave-lengths), of inviscid wave-interaction instability when the 'more viscous' fluid has the greater velocity. This is seen as a second hump on the right in figure 15(b). Being a short wave-length mode, it is suppressed by viscosity.

We now have an instability caused by the interaction of three waves sitting on three vorticity-jump interfaces. Wave-interaction must be dependent on the separation between interfaces. To investigate this, we plot the dominant growth rate of the longer wave mode as a function of the location h of the slope change in figure 16. As in the viscous case it is seen that the location of the interface does matter and the trend is broadly in agreement with viscous results.

Having demonstrated the effect of wave-interaction, we return to the viscous case in the rest of the paper, this time to perform a spatio-temporal stability analysis.

3.3. *Spatio-temporal stability analysis for the viscous flow*

In order to understand the nature of instability, i.e, whether the flow is absolutely or convectively unstable, we follow the Briggs (1964) approach, as is fairly standard now. It has been used in mixing layers, jets and wakes, and in plasma flows (see for instance,

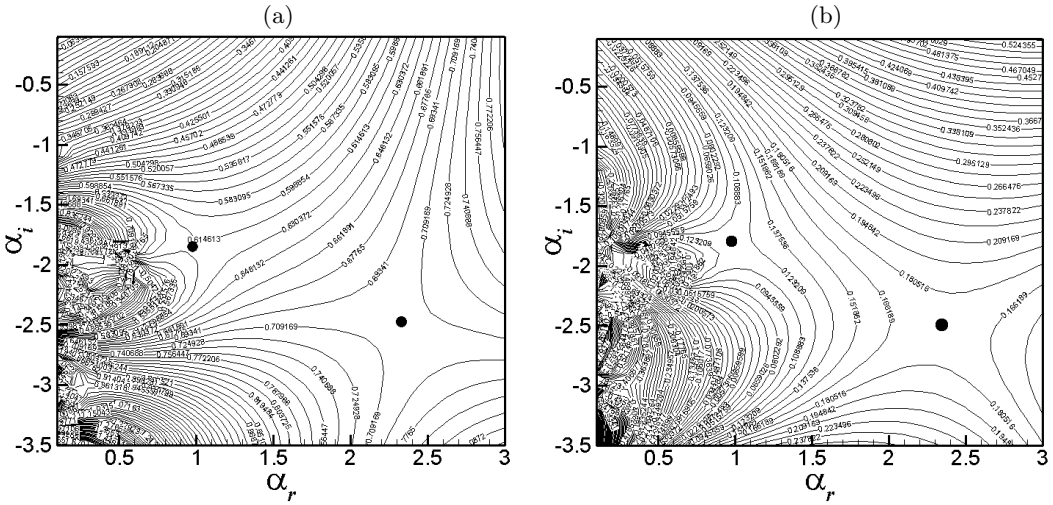

FIGURE 17. Isocontours of (a) ω_r and (b) ω_i in the complex wavenumber plane. The parameters are $\mathrm{Re} = 100$, $R_s = -1$, $R_t = 2$, $h = 0.5693$, $q = 0.1138$. The value of the complex frequency ω_0 at the top and bottom saddle points (shown by filled circles) are $0.616 + 0.118\mathrm{i}$ and $0.706 + 0.174\mathrm{i}$ respectively.

Bers (1983); Huerre & Monkewitz (1990); Vihinen *et al.* (1997); Criminale *et al.* (2003); Chomaz (2005); Kaiktsis & Monkewitz (2003)), and in miscible and immiscible channel flow [Sahu & Govindarajan (2012); Sahu & Matar (2011); Selvam *et al.* (2009)]. The procedure is briefly outlined below for completeness.

The linearised differential operator given by Eqs. (2.14) and (2.15) represents a dispersion relation, $\omega_i = \omega_i(\alpha; \mathrm{Re}, \mathrm{Sc}, R_s, R_t, h, q)$ in complex (ω, α) space. Note that in the spatio-temporal stability analysis both wave-number and frequency of the disturbance are complex. To obtain the response of the linearised system to an impulse perturbation, we may introduce the corresponding Green's function, $G(x, y, t)$. For a given mode, the long-time behaviour of G is then obtained along different 'rays', which correspond to different constant values of x/t. The value of x/t also corresponds to the group velocity of the mode, i.e.,

$$\frac{x}{t} = \frac{\partial \omega}{\partial \alpha}(\alpha). \tag{3.1}$$

In order to determine whether the flow is convectively or absolutely unstable, one calculates the so-called absolute frequency $\omega_0 = \omega(\alpha_0)$, corresponding to the complex 'absolute wavenumber' α_0, which satisfies

$$\frac{\partial \omega}{\partial \alpha}(\alpha_0) = 0. \tag{3.2}$$

Thus this corresponds to the ray $x/t = 0$, which has a zero group velocity. Flow is said to be absolutely unstable if the absolute growth rate (imaginary part of ω_0), $\omega_{0i} > 0$. In this case, we have an impulse response growing locally, and usually spreading both upstream and downstream from its source. On the other hand, flow is convectively unstable, i.e the impulse disturbances grow as they move downstream from their source, if $\omega_{0i} < 0$ but $\omega_i > 0$ for some mode.

As discussed above, the unstratified case was studied in the inviscid limit by Huerre & Monkewitz (1985) and shown to be absolutely unstable above a certain velocity ratio R_t. A value of $R_t = 2$, which is absolutely unstable in the unstratified case, is chosen for comparison. Contours of constant frequency and growth rate for the case $R_s = -1$ are

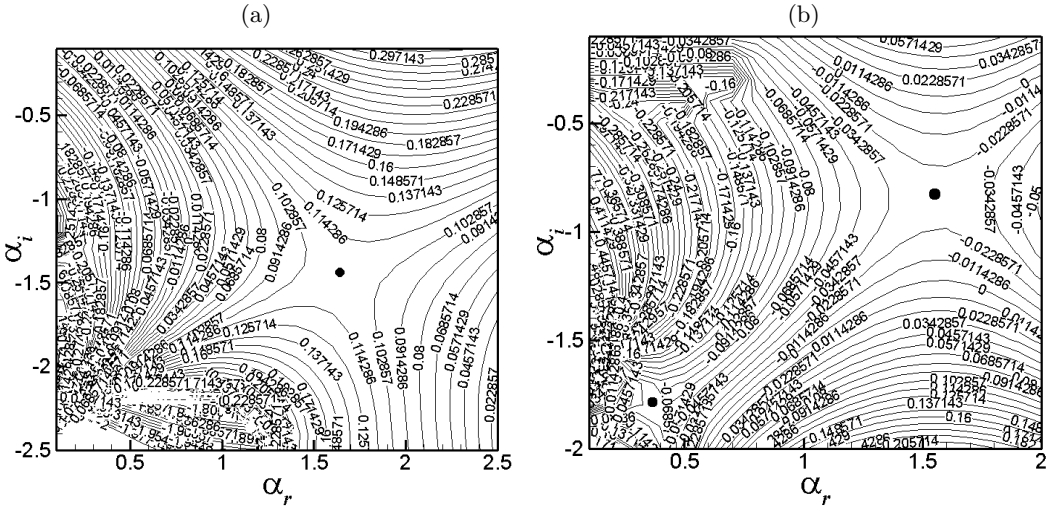

FIGURE 18. Isocontours of ω_i in the complex wavenumber plane for (a) The unstratified case, $R_s = 0$. At the saddle point (filled circle), $\omega_{0i} = 0.108$. (b) $R_s = 1$. $\omega_{0i} = -0.026$ and -0.071 at the top and bottom saddle points (shown by filled circles), respectively. The values of the rest of the parameters are Re = 100, $R_t = 2$, $h = 0.5693$, $q = 0.1138$.

shown in figure 17. Figure 17(b) may be contrasted with the unstratified result shown in figure 18(a). The growth rates are bigger with $R_s = -1$. Stratification gives rise to two saddle points in the same vicinity, as opposed to a single one in the case of unstratified flow. Among the two saddle points, the one lying on top is the only relevant one for absolute instability. The other saddle point satisfies the criterion of $\omega_i > 0$, but the upper and lower branches of the contours contours both begin from the negative α_i part of the plane, which does not satisfy the additional requirement for absolute instability (Briggs 1964) that upstream and downstream propagating branches must lie different half-planes. The other saddle point results from a coalescence produced at the true pinch point. This is reminiscent of the multiple saddle points seen in confined unstratified shear layers by Juniper (2006); in that case too not all saddle points were indicative of absolute instability. Detailed numerical simulations, to follow into the nonlinear regime the consequences of the absolutely growing mode, will be interesting. In the 'stabilized' stratification of $R_s = 1$, we see (figure 18b) that the absolute growth rate has decreased a lot. Again stratification introduces an additional saddle point, but this has a negative value of ω_{i0}.

The effect of the velocity ratio $R_t\,[\equiv (U_\infty - U_{-\infty})/(U_\infty + U_{-\infty})]$ on the stability is summarized in figure 19. All cases are absolutely unstable above a certain R_t, and $R_s = 1$ is significantly stabilized overall, both in terms of the critical R_t and the absolute growth rate. It can be seen that $R_s = -1$ is destabilized, consistent with the convective stability behavior. We had seen earlier that the location of the viscosity interface made a difference to the convective growth rates. What about the absolute instability? Growth rates at the saddle points are shown for the case $R_s = -1$ in figure 20(a) at different locations of the viscosity interface. The concentration profile which results from placing the interface at a given h is provided in figure 20(b). The absolute growth rates are largest for small h, which means that the most dangerous location to place the viscosity stratification is the middle of the shear layer.

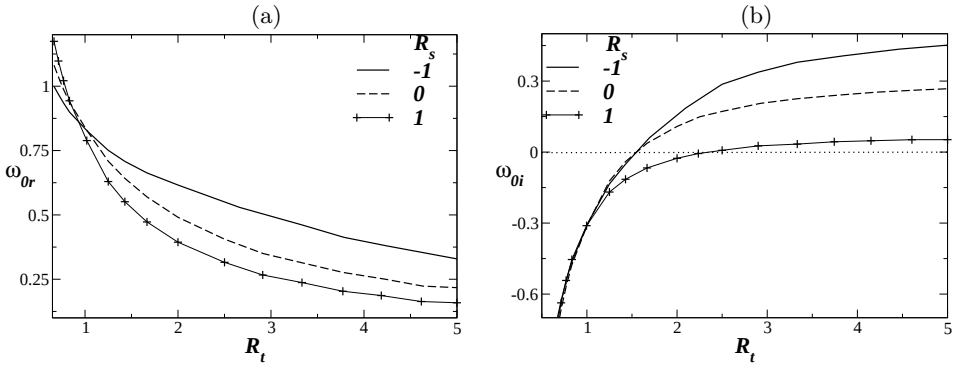

FIGURE 19. Frequency and growth rate of the zero group velocity mode, as a function of the velocity ratio, for three values of R_s. As before, Re = 100, $h = 0.5693$, $q = 0.1138$. Values of $\omega_{0i} > 0$ indicate absolute instability.

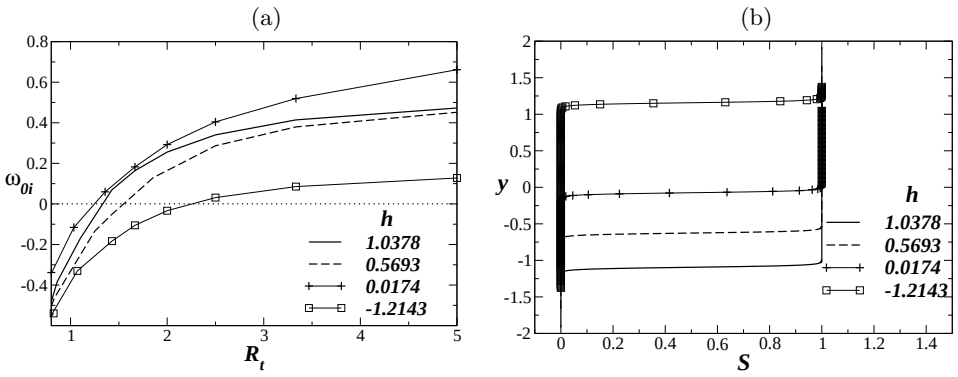

FIGURE 20. (a) Variation of ω_{0i} with velocity ratio for different locations of the viscosity interface. $R_s = -1$, Re = 100, Sc = 1, $q = 0.1138$. (b) The corresponding basic profiles of concentration S.

4. Conclusions

We have discussed two geophysical situations in which a layer of viscosity stratification is proximate to a shear layer, but these situations are likely to be common in many other situations of interest. For example in the Earth's outer core, simulations [Gubbins *et al.* (2011), Sreenivasan, private communication] reveal such flows. The main objective of this paper has been to show that viscosity stratification, often ignored in such studies, can affect both instability growth rates and the dominant wavenumbers significantly. Ocean-floor patterns formed by settling of turbidity currents are a function of how fast and at what spacing debris is deposited. An interesting revelation has been that the mixing layer is affected in ways different from other shear flows. In particular, the diffusivity of one species into the other makes no difference to the result. This will be very surprising for those who have worked with viscosity stratification in the context of channel and pipe flows, where diffusivity is one of the most important quantities deciding stability.

The broad qualitative agreement between viscous and model inviscid results is one indication that an inviscid non-diffusive mechanism has a role to play, via a change in the velocity profile above and below the stratified layer. We note however that the viscous problem is more complex, and the analogy is incomplete. In particular, the destabilization of stabilization achieved is a non-monotonic effect peaking when the stratified layer and

the shear layer have a significant overlap, but their centers are some distance apart, i.e., in a region where viscous effects are important.

We have seen that by choosing viscosity stratification carefully, a stabilization of the absolute disturbance growth can be achieved as well.

Acknowledgments: The authors thank Manoj Tripathi for help in making a few sketches for this paper. The anonymous referees are thanked for useful suggestions. This work is partially supported by the Ministry of Earth Sciences, Government of India, under the Monsoon Mission Project on the Bay of Bengal.

Appendix A. Base state velocity profile

We start the derivation from the steady state, boundary layer equations Burridge & Drazin (1969), given by

$$u\frac{\partial u}{\partial \zeta} + v\frac{\partial u}{\partial \eta} = \frac{\partial}{\partial \eta}\left(\nu \frac{\partial u}{\partial \eta}\right), \tag{4.1}$$

$$\frac{\partial u}{\partial \zeta} + \frac{\partial v}{\partial \eta} = 0, \tag{4.2}$$

where ζ and η are the original horizontal and transverse directions, respectively. Then by transforming the equations to a single-dimensionless variable, y, given by

$$y = \eta \left(\frac{\rho_0 U_\infty}{\mu_{-\infty}\zeta}\right)^{1/2}, \tag{4.3}$$

we obtain

$$f''' + \frac{1}{2\mu_0} f f'' + \frac{\mu_0'}{\mu_0} f'' = 0. \tag{4.4}$$

Here $\mu_{-\infty}$ is the viscosity of the fluid at $y = -\infty$. It is to be noted that Re does not appear in this equation.

Appendix B. Stability equations for the inviscid model

The governing system of stability equations for the inviscid model are:

$$AX = cBX, \tag{4.5}$$

where X represents the eigenfunctions, The matrices A and B are given by

$$\begin{bmatrix} 2\alpha U_\infty - s_1 & -s_1 e^{-2k} & 0 & 0 \\ 1 & e^{-2\alpha\mathcal{H}} & -1 & e^{-2\alpha\mathcal{H}} \\ 2\alpha U_\infty - s_1 + s_2 & (s_2 - s_1)e^{-2\alpha\mathcal{H}} & -2\alpha U_\infty & 2\alpha U_{-\infty} \\ 0 & 0 & s_2 e^{-2\alpha} & 2\alpha U_{-\infty} + s_2 \end{bmatrix}, \quad \text{and} \tag{4.6}$$

$$\begin{bmatrix} 2\alpha & 0 & 0 & 0 \\ 0 & 0 & 0 & 0 \\ 2\alpha & 0 & -2\alpha & 0 \\ 0 & 0 & 0 & 2\alpha \end{bmatrix}, \tag{4.7}$$

respectively, where $\mathcal{H} = \left(e^{-R_s} - 1 - 2he^{-R_s}\right)/\left(1 + e^{-R_s}\right)$. These equations are obtained by implementing decaying conditions in each free stream, and continuity of streamfunction and normal stresses at each interface:

$$\psi_+ = \psi_-, \quad \text{and} \quad {\psi'}_+ - {\psi'}_- = [{U'}_+ - {U'}_-]\,\psi, \tag{4.8}$$

wherein, subscripts + and − designate locations just above and just below each interface.

REFERENCES

Bague, A., Fuster, D., Popinet, S., Scardovelli, R. & Zaleski, S. 2010 Instability growth rate of two-phase mixing layers from a linear eigenvalue problem and an initial-value problem. *Phys. Fluids* **22**, 092104.

Bers, A. 1983 Space-time evolution of plasma instabilities - absolute and convective. In *Handbook of Plasma Physics* (ed. M. N. Rosenbluth & R. Z. Sagdeev) **1**, 451–517. North Holland: North-Holland Publishing Company, Amsterdam.

Betchov, R. & Szewczyk, A. 1963 Stability of a shear layer between parallel streams. *Phys. Fluids* **6(10)**, 1391–1396.

Bhattacharya, P., Manoharan, M. P., Govindarajan, R. & Narasimha, R. 2005 The critical Reynolds number of a laminar incompressible mixing layer from minimal composite theory. *J. Fluid Mech.* **565**, 105–114.

Biancofiore, L. & Gallaire, F. 2012 Counterpropagating roassby waves in confined plane wakes. *Phys. Fluids* **24**, 074102.

Bishop, C. H. & Heifetz, E. 2000 Apparent absolute instability and the continuous spectrum. *J. Atmos. Sc.* **57**, 3592–3608.

Boeck, T. & Zaleski, S. 2005 Viscous versus inviscid instability of two-phase mixing layers with continuous velocity prole. *Phys. Fluids* **17**, 032106.

Briggs, R. J. 1964 *Electron-stream interaction with plasmas, Research monograph no. 29*. Cambridge: MIT Press.

Burridge, D. M. & Drazin, P. G. 1969 Comments on stability of pipe Poiseuille flow. *Phys. Fluids* **12**, 264–265.

Carpenter, J. R., Balmforth, N. J. & Lawrence, G. A. 2010 Indetifying unstable modes in stratified shear layers. *Phys. Fluids* **22**, 054104.

Caulfield, C. P. 1994 On the behaviour of symmetric waves in stratified shear layers. *J. Fluid Mech.* **258**, 255–285.

Chomaz, J.-M. 2005 Global instabilities in spatially developing flows: non-normality and nonlinearity. *Ann. Rev. Fluid Mech.* **37**, 357–392.

Craik, A. D. D. 1985 *Wave Interactions and Fluid Flows*. New Your: Cambridge University Press.

Criminale, W. O., Jackson, T. L. & Roslin, R. D. 2003 *Theory and Compuation of Hydrodynamic Stability*. Cambridge, UK: Cambridge University Press.

Drazin, P. G. & Reid, W. H. 1985 *Hydrodynamic stability*. Cambridge: Cambridge University Press.

Ern, P., Charru, F. & Luchini, P. 2003 Stability analysis of a shear flow with strongly stratified viscosity. *J. Fluid Mech.* **496**, 295-312.

Govindarajan, R 2004 Effect of miscibility on the linear instability of two-fluid channel flow. *Int. J. Multiphase Flow* **30**, 1177–1192.

Govindarajan, R., L'vov, S. V. & Procaccia, I. 2001 Retardation of the onset of turbulence by minor viscosity contrasts. *Phys. Rev. Lett.* **87**, 174501.

Govindarajan, R. & Sahu, K. C. 2014 Instabilities in viscosity-stratified flows. *Ann. Rev. Fluid Mech.* **46**, 331–353.

Gubbins, D., Sreenivasan, B., Mound, J. & Rost, S. 2011 Melting of the earths inner core. *Nature* **473**, 361–363.

Harnik, N., Heifetz, E., Umurhan, O. M. & Lott, F. 2006 A buoyancy-vorticity wave interaction approach to stratified shear flow. *J. Atmos. Sci.* **65**, 2615–2630.

Healey, J. J. 2009 Destabilising effects of confinement on homogeneour mixing layers. *J. Fluid Mech.* **623**, 241–271.

Heifetz, E. & Methven, J. 2005 Relating optimal growth to counterpropagating rossby waves in shear instability. *Phys. Fluids* **17**, 064107.

Heifetz, E., Reuveni, Y., Gelfgat, A., Kit, E. & Methven, J. 2006 The counterpropagating rossby wave perspective on kelvin helmholtz instability as a limiting case of a rayleigh shear layer with zero width. *Phys. Fluids* **18**, 018101.

Hinch, E. J. 1984 A note on the mechanism of the instability at the interface between two shearing fluids. *J. Fluid Mech.* **144**, 463–465.

Hooper, A. P. & Boyd, W. G. C. 1983 Shear flow instability at the interface between two fluids. *J. Fluid Mech.* **128**, 507–528.

Huerre, P. & Monkewitz, P. A. 1985 Absolute and convective instabilities in free shear layers. *J. Fluid Mech.* **156**, 151–168.

Huerre, P. & Monkewitz, P. A. 1990 Local and global instability in spatially developing flows. *Ann. Rev. Fluid Mech.* **22**, 473–537.

Huerre, P. & Rossi, M. 1998 Hydrodynamic instabilities in openflows. In *Hydrodynamics and nonlinear instabilities* (ed. C. Godreche & P. Manneville), pp. 81–288. The Pitt Building, Trumpington Street, Cambridge CB21RP, United Kingdom: Cambridge University Press.

Juniper, M. P. 2006 The effect of confinement on the stability of two-dimensional shear flows. *J. Fluid Mech.* **565**, 171–195.

Kaiktsis, L & Monkewitz, P. A. 2003 Global destabilization of flow over a backward-facing step. *Phys. Fluids* **15 (12)**, 3647–3658.

McIntyre, M. E. 2013 Rossby-wave propagation and shear instability (appendix 1). *GEFD Summer school, Cambridge* .

Mishra, M., De Wit, A. & Sahu, K. C. 2012 Double diffusive effects on pressure-driven miscible displacement flows in a channel. *J. Fluid Mech.* **712**, 579–597.

Nasr-Azadani, Hall, B, M., M. & Meiburg, E. 2013 Polydisperse turbidity currents propagating over complex topography: Comparison of experimental and depth-resolved simulation results. *Comp. & Geosc.* **53**, 141–153.

Nasr-Azadani, M. M. & Meiburg, E. 2014 Turbidity currents interacting with three-dimensional seaoor topography. *J. Fluid Mech.* **745**, 409–443.

Ranganathan, B. T. & Govindarajan, R. 2001 Stabilisation and destabilisation of channel flow by location of viscosity-stratified fluid layer. *Phys. Fluids.* **13(1)**, 1–3.

Robinet, J. C & Dussauge, J. C. 2001 Wall effect on the convectiveabsolute boundary for the compressible shear layer. *Theoret. Comput. Fluid Dynamics* **15**, 143–163.

Sahu, K. C., Ding, H., Valluri, P. & Matar, O. K. 2009 Linear stability analysis and numerical simulation of miscible channel flows. *Phys. Fluids* **21**, 042104.

Sahu, K. C. & Govindarajan, R. 2012 Spatio-temporal linear stability of double-diffusive two-fluid channel flow. *Phys. Fluids* **24**, 054103.

Sahu, K. C. & Matar, O. K. 2011 Three-dimensional convective and absolute instabilities in pressure-driven two-layer channel flow. *Int. J. Multiphase Flow* **37**, 987–993.

Schaflinger, U. 1994 A short note on Squires theorem for interfacial instabilities in a stratified flow of two superposed fluids. *Fluid Dyn. Res.* **14**, 223–227.

Schmid, P. J. & Henningson, D. S. 2001 *Stability and Transition in Shear Flows*. New York: Springer.

Selvam, B., Talon, L., Lesshafft, L. & Meiburg, E. 2009 Convective/absolute instability in miscible core-annular flow. part 2. numerical simulations and nonlinear global modes. *J. Fluid Mech.* **618**, 323–348.

Usha, R., Tammisola, O. & Govindarajan, R. 2013 Linear stability of miscible two-fluid flow down an incline. *Phys. Fluids* **25**, 104102.

Vihinen, I, Honohan, A. M. & Lin, S. P. 1997 Image of absolute instability in a liquid jet. *Phys. Fluids* **9 (11)**, 3117–3119.

Wilson, H. J. & Rallison, J. M. 1999 Instability of channel flows of elastic liquids having continuously stratified properties. *J. Non-Newt. Fluid Mech.* **85**, 273–298.

Yecko, P. & Zaleski, S. 2005 Transient growth in two-phase mixing layers. *J. Fluid Mech.* **528**, 43–52.

Yih, C. S. 1955 Stability of of two-dimensional parallel flows for three dimensional disturbances. *Quart. Appl. Math.* **12**, 434–435.

Yih, C. S. 1967 Instability due to viscous stratification. *J. Fluid Mech.* **27**, 337–352.